Interpolated Joint Space Adversarial Training for Robust and Generalizable Defenses

Chun Pong Lau¹, Jiang Liu¹, Hossein Souri¹, Wei-An Lin², Soheil Feizi³, Rama Chellappa¹ Johns Hopkins University, ²Adobe, ³University of Maryland, College Park

{jliu214, clau13, hsouri1, rchella4}@jhu.edu, walin@umd.edu, sfeizi@cs.umd.edu

Abstract

Adversarial training (AT) is considered to be one of the most reliable defenses against adversarial attacks. However, models trained with AT sacrifice standard accuracy and do not generalize well to novel attacks. Recent works show generalization improvement with adversarial samples under novel threat models such as on-manifold threat model or neural perceptual threat model. However, the former requires exact manifold information while the latter requires algorithm relaxation. Motivated by these considerations, we exploit the underlying manifold information with Normalizing Flow, ensuring that exact manifold assumption holds. Moreover, we propose a novel threat model called Joint Space Threat Model (JSTM), which can serve as a special case of the neural perceptual threat model that does not require additional relaxation to craft the corresponding adversarial attacks. Under JSTM, we develop novel adversarial attacks and defenses. The mixup strategy improves the standard accuracy of neural networks but sacrifices robustness when combined with AT. To tackle this issue, we propose the Robust Mixup strategy in which we maximize the adversity of the interpolated images and gain robustness and prevent overfitting. Our experiments show that Interpolated Joint Space Adversarial Training (IJSAT) achieves good performance in standard accuracy, robustness, and generalization in CIFAR-10/100, OM-ImageNet, and CIFAR-10-C datasets. IJSAT is also flexible and can be used as a data augmentation method to improve standard accuracy and combine with many existing AT approaches to improve robustness.

1. Introduction

Although recent research has shown that neural networks are highly successful in various applications [15,19,25,32], they are vulnerable to adversarial samples which are intentionally designed to fool the model [2, 3, 5, 13, 16]. This poses a massive challenge in security-critical applications such as autonomous driving [26] and medical imaging [1].

To tackle this problem, several defense methods have

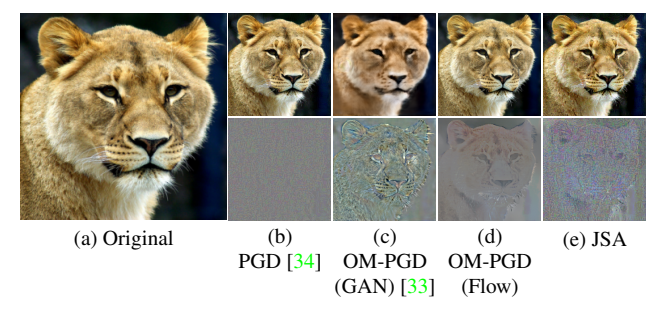


Figure 1. Visualization of adversarial samples from AT [34], OM-PGD (GAN) [33], OM-PGD (Flow) and our proposed JSA.

Robust Accuracy against PGD Attack

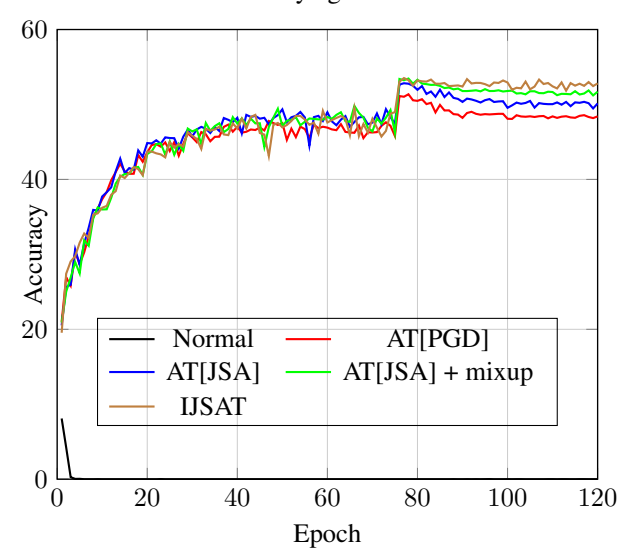


Figure 2. PGD robustness during training with CIFAR-10 dataset. Using JSA with AT, we can observe a significant improvement. Using normal mixup with it, we can see further improvement but also observe robust overfitting after the learning rate changes (at 75^{th} epoch). IJAST has better robustness and does not have robustness drop after learning rate changes.

been proposed including empirical and certifiable defense methods [7, 8, 31, 32, 37, 39, 42, 43, 48, 52, 54]. In Adversarial Training, the defender generates adversarial samples

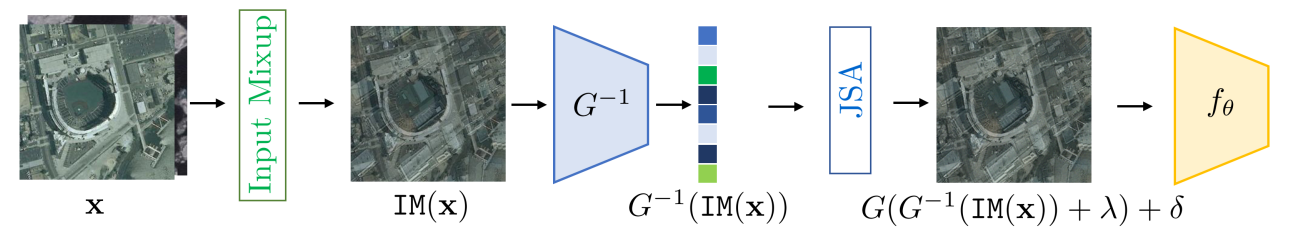


Figure 3. The overall pipeline of the proposed Interpolated Joint Space Adversarial Training (IJSAT). First, Input Mixup is applied to two images to get an interpolated image. Then it is passed to the Flow-based Model to get the latent vector. We apply the proposed Joint Space Attack to it and get the adversarial sample. Finally, we pass it to the classifier. During test time, images are directly passed to the adversarially trained classifier.

that obey a certain threat model and utilizes them in the training process in order to get a robust model [34]. In other words, existing AT methods consider perturbed samples, for example, within a small L_p norm-bound distance and assure robustness to the same type of perturbed samples. However, models trained using AT suffer from not being robust to novel imperceptible attacks [27,28,38,46]. In addition, it has been observed that AT can often cause a reduction in standard accuracy, i.e., the accuracy on clean data, which indicates that a trade-off between robustness and accuracy [34,40,47,58] is at play. To further improve robustness, one usually trains models by AT with a larger attack budget. Although this improves robustness, the standard accuracy of the models is sacrificed.

Recently, several works aim to use a low-dimensional underlying data manifold to attack neural networks by creating on-manifold adversarial samples [20, 33, 46, 47]. Onmanifold adversarial samples are adversarial samples constrained to lie on data manifolds and are obtained by perturbing inputs in the latent space learned by generative models. Adversarial samples computed in the image space are considered as off-manifold [47]. On-manifold adversarial samples have been used to break models trained by AT [46] as well as deep generative model-based defense methods [6] such as DefenseGAN [43], Analysis by Synthetics [44] and MoG-VAE [14]. In response to this attack, several manifold-based defense methods have been proposed lately [20, 33, 47]. [20] takes advantage of the low-dimensional data manifold and introduces a sup player, which is more powerful than regular adversarial training. [47] shows that robustness against on-manifold adversarial samples is related to the generalization ability of neural networks and proposes on-manifold adversarial training. [33] investigates the scenario that the manifold hypothesis holds (i.e. exact information about the underlying data manifold is given) and proposes dual manifold adversarial training (DMAT), which utilizes both on-manifold and off-manifold adversarial samples to robustify the models. The authors show that DMAT can improve model robustness against L_p and non- L_p attacks. However, DMAT only considers on-manifold images during both training and testing while in practice, the testing images are natural (off-manifold) images.

Interpolation-based training has been recently proposed in several works [29, 30, 37, 50, 57], which can improve the generalization and robustness properties of neural networks. [57] has introduced a data augmentation routine called input mixup in which two data samples are drawn from the training dataset, and a linear interpolation of the samples is passed through the network with the loss computed using the same linear interpolation of losses. The manifold mixup as a regularization tool uses the interpolation of the hidden representations of a randomly selected layer [50]. Interpolated adversarial training (IAT) [29] proposes to employ either input mixup or manifold mixup combined with AT to benefit from both interpolated and AT methods and improves generalization while preserving robustness. However, IAT interpolates images after perturbation such that the interpolated images are not guaranteed to mislead the classifier.

In this paper, we focus on developing a classifier with good standard accuracy, robust to seen attacks, and generalizing well to unseen attacks. To overcome the inability of L_p adversarial samples to maintain standard accuracy and the on-manifold adversarial samples' ineffectiveness in defending the L_p attacks, we propose a novel threat model called Joint Space Threat Model (JSTM) that perturbs images in both image space and latent space (See Fig. 1(e)). To ensure that on-manifold adversarial samples generalize well, which requires the exact manifold assumption, we use an invertible Flow-based model to guarantee generalizability. (See Fig. 1(d)). To prevent robust overfitting [41] and further improve robustness generalization, we propose a Robust Mixup strategy in which we attack the interpolated samples directly to increase their adversity and hence achieve better robustness (See Fig. 2). In light of these, we propose Intepolated Joint Space Adversarial Training (IJSAT), which applies Robust Mixup strategy and trains the model with JSA samples. The overall pipeline is shown in Fig. 3.

Contributions:

We propose Joint Space Attack (JSA), which simultaneously optimizes the perturbations in image space and la-

tent space. We empirically show JSA samples are robust to both L_p attacks and unseen attacks.

- We propose the Robust Mixup strategy, which can further improve robustness and generalization and prevent overfitting.
- We empirically demonstrate that IJAST achieves good performance in both standard accuracy, robustness, and generalization in CIFAR-10, CIFAR-100, OM-ImageNet, and CIFAR-10-C datasets.
- IJAST can also serve as a data augmentation method to improve the standard accuracy of the classifiers and assist with other AT methods to achieve better robustness.

2. Mathematical Background

2.1. Setup

We consider the multi-class classification problem, where the image samples $x \in \mathcal{X} := \mathbb{R}^{H \times W \times C}$ are drawn from an underlying distribution \mathbb{P}_X , where H,W and C are the height, width and the number of channels of the image respectively. Let f_θ be a parameterized model which maps any image in \mathcal{X} to a discrete label y in $\mathcal{Y} := \{1, \cdots, |\mathcal{Y}|\}$. An accurate classifier maps an image x to its corresponding true label y_{true} , i.e. $f_\theta(x) = y_{\text{true}}$. A successful attack fools the classifier to map an adversarial image \hat{x} to a wrong label, i.e. $f_\theta(\hat{x}) \neq y_{\text{true}}$. We define the manifold information to be exact, when there exists a generative model G such that there exists a latent representation z for every image x.

Definition 1 (Exact Manifold Assumption). Fix a generator G.

$$\forall x \in \mathcal{X}, \ \exists z \in Z \ s.t. \ G(z) = x.$$

2.2. Standard and On-Manifold Robustness

We consider off-manifold adversarial samples \hat{x}^{img} and on-manifold adversarial samples \hat{x}^{lat} in the context of standard adversarial robustness and on-manifold adversarial robustness respectively. Both \hat{x}^{img} and \hat{x}^{lat} are visually indistinguishable from x. To create perturbations in image space \mathcal{X} and latent space Z, we consider the popular L_p additive attacks where $\hat{x}^{img} = x + \delta$ and $\hat{x}^{lat} = G(z + \lambda)$ where $z \in Z$ is the corresponding latent vector. Formally,

$$\max_{\delta \in \Delta} \mathcal{L}(f_{\theta}(x+\delta), y_{\text{true}}), \tag{1}$$

and

$$\max_{\lambda \in \Lambda} \mathcal{L}(f_{\theta}(G(z+\lambda)), y_{\text{true}}), \tag{2}$$

where $\Delta = \{\delta : \|\delta\|_p < \epsilon\}$, $\Lambda = \{\lambda : \|\lambda\|_p < \eta\}$ and $\mathcal L$ is a classification loss function (e.g. the cross-entropy loss). In our work, we focus on $p = \infty$, and will explicitly specify when $p \neq \infty$. In (1), since the function is non-convex, the maximization is typically performed using

gradient-based optimization methods. In this paper, we consider the PGD attack and use the notation PGD-K to represent K-step PGD attacks with bounded L_{∞} norm.

To defend against norm-bounded attacks, an established AT approach by Madry *et al.* [34] considers the following min-max formulation:

$$\min_{\theta} \sum_{i} \max_{\delta \in \Delta} \mathcal{L}(f_{\theta}(x_i + \delta), y_{\text{true}}), \tag{3}$$

where the classification model f_{θ} is trained exclusively on adversarial images by minimizing the cross-entropy loss. In a similar manner, we can defend the on-manifold adversarial samples which are crafted by OM-PGD attack by

$$\min_{\theta} \sum_{i} \max_{\lambda \in \Lambda} \mathcal{L}(f_{\theta}(G(z_i + \lambda)), y_{\text{true}}). \tag{4}$$

2.3. Flow-Based Generative Model

Suppose Z is a random variable with an explicit and tractable probability function (pdf) $p_Z:Z\to\mathbb{R}$. Let G be an invertible function and X=G(Z). By change of variables equation, the pdf of X:

$$p_X(x) = p_Z(G^{-1}(x)) |\det DG^{-1}(x)|$$

= $p_Z(G^{-1}(x)) |\det DG(G^{-1}(x))|^{-1}$, (5)

where G^{-1} is the inverse of G, $\mathrm{D}G(z)=\frac{\partial G}{\partial z}$ is the Jacobian of G and $\mathrm{D}G^{-1}(x)=\frac{\partial H}{\partial x}$ is the Jacobian of G^{-1} .

Although GANs largely dominate generative models, one major drawback of GANs is that they cannot compute the exact sample likelihoods. Flow-based generative models solve this problem by having an invertible function that has the properties mentioned above. The invertible function G is typically modeled as the composition of K invertible maps, i.e. $G = G_1 \circ G_2 \circ \cdots \circ G_K$. This is also called the *normalizing flows* [11]. Different designs for constructing G have been proposed in recent years. NICE [11] uses coupling layers to enable highly expressive transformation for flows. RealNVP [12] uses affine coupling layers which basically represent invertible scale transformations. Glow [22] uses invertible 1×1 convolutions to have learnable permutations.

2.4. Mixup Strategy

Overfitting usually occurs when models are adversarially trained. This leads to the degradation of standard accuracy and generalization. To mitigate this drawback while preserving certain robustness, interpolation-based training techniques [29, 37, 50, 57] are adopted, which are shown to be effective and have demonstrated promising performance in adversarial robustness and generalization improvements. In our work, we focus on using Input Mixup [57] to combine the off-manifold and on-manifold adversarial samples. Input Mixup draws two pairs of data sample from

the dataset, (x_i,y_i) , $(x_j,y_j) \sim \mathbb{P}_X$, and takes the convex combination between them in the image space $\mathrm{IM}(\mathbf{x}) = \alpha x_i + (1-\alpha)x_j$, where IM is the Input Mixup function, $\mathbf{x} = (x_i,x_j)$ is the pair of images and $\alpha \in (0,1)$ is a random variable with Beta distribution. The interpolated image $\mathrm{IM}(\mathbf{x})$ is passed into the classifier f_θ with minimizing the convex combination of the cross-entropy loss,

$$\mathcal{L}_{\alpha}^{mix}(\mathtt{IM}(\mathbf{x})) = \alpha \mathcal{L}(f_{\theta}(\mathtt{IM}(\mathbf{x})), y_i) + (1 - \alpha) \mathcal{L}(f_{\theta}(\mathtt{IM}(\mathbf{x})), y_i).$$
 (6)

3. Joint Space Threat Model

The ideal robust classifier should have the following properties: 1) Good standard accuracy; 2) Robust to seen attacks/known threat model; 3) Generalized to unseen attacks. AT provides satisfactory robustness to known threat models while sacrificing 1) and 3). To achieve 3), one can craft adversarial samples under a more comprehensive threat model. [35] considers the union of threat models by having average or maximum of the adversarial samples. However, it is not robust with adversarial attacks outside the union of threat model and computationally costly as it crafts each adversarial sample under the threat model within the union. [33] considers on-manifold adversarial samples, which improve standard accuracy and generalize to unseen attacks, but it requires exact manifold information. [28] considers a comprehensive threat model called Neural Perceptual Threat Model (NPTM), which improves robustness to unseen attacks but sacrifices standard accuracy and requires additional relaxation in the attack algorithm.

In light of these, we propose the Joint Space Threat Model (JSTM), which considers both image and latent space perturbations in one adversarial sample. To obtain a wider threat model, we consider the combination of image and latent space perturbations instead of considering the union of threat model and having a larger parameter space, i.e. $\Delta \cup \Lambda$. Mathematically, JSTM can be expressed as

$$\max_{\delta \in \Delta, \lambda \in \Lambda} \mathcal{L}(f_{\theta}(G(G^{-1}(x) + \lambda) + \delta), y_{\text{true}}) \tag{7}$$

where G is Flow-based model. Since G is invertible, exact manifold assumption holds. Moreover, JSTM is a special case of NPTM which does not require additional relaxations to craft adversarial attack.

Lemma 1. Assume image space perturbation $\delta=0$. Then JSTM is NPTM with the neural perceptual distance $\phi=G^{-1}$.

Proof.
$$\max_{\hat{x}} \mathcal{L}(f_{\theta}(\hat{x}), y_{\text{true}}) \ s.t. \ \|G^{-1}(\hat{x}) - G^{-1}(x)\| < \eta$$

$$\iff \max_{\lambda} \mathcal{L}(f_{\theta}(G(z + \lambda)), y_{\text{true}})$$

$$s.t. \ \|G^{-1}(G(z + \lambda)) - G^{-1}(G(z))\| < \eta$$

$$\iff \max_{\lambda \in \Lambda} \mathcal{L}(f_{\theta}(G(z + \lambda)), y_{\text{true}})$$

The second line holds as G is invertible so for any \hat{x} , there exists λ such that $G(z + \lambda) = \hat{x}$.

To optimize (7), we propose the Joint Space Attack (JSA) algorithm, which uses the sign of gradients to update the λ and δ similar to PGD attacks. Given an initial latent vector $z = G^{-1}(x)$, we have

$$\lambda_{k+1} = \eta_{iter} \cdot sign\left(\nabla_{\lambda_k} \mathcal{L}(f_{\theta}(G(z + \lambda_k) + \delta_k), y_{\text{true}})\right),$$

$$\delta_{k+1} = \epsilon_{iter} \cdot sign\left(\nabla_{\delta_k} \mathcal{L}(f_{\theta}(G(z + \lambda_k) + \delta_k), y_{\text{true}})\right),$$

(8)

where ϵ_{iter} and η_{iter} are the attack step size at each iteration for image space and latent space, respectively. Also, there is a constraint on the JSA adversarial samples $\hat{x} = \text{clip}(G(z+\lambda)+\delta)$ within the image range, i.e. $\hat{x} \in \mathcal{X}$ and clip is the clip operator to clip the image within the range. Since we leverage the flow-based model, no additional relaxation is needed, while Perceptual Projected Gradient Descent (PPGD) under NPTM needs Taylor's approximation.

4. Optimized Perturbation with Interpolated Images

To achieve better standard accuracy, one can use data augmentation. Input mixup is one of the popular data augmentation methods, and it is easy to combine with AT. Interpolated Adversarial Training (IAT), proposed by [29], combines AT and interpolation-based training to design a robust classifier. A mixture of clean perturbed images is used in IAT. Although IAT demonstrates certain adversarial robustness, it is not optimized from a mathematical perspective in that the interpolated images are not guaranteed to maximize the cross-entropy loss. Suppose x_i, x_j are two images, y_i, y_j are the corresponding labels and $\text{IM}(\mathbf{x}) = \alpha x_i + (1-\alpha)x_j$ be the interpolated image. Let \hat{x}_i^{img} and \hat{x}_j^{img} be the perturbed image with perturbation δ_i and δ_j respectively. The interpolated perturbation need not be the optimized perturbation w.r.t the interpolated image $\text{IM}(\mathbf{x})$ as,

$$\begin{split} \text{IM}(\hat{\mathbf{x}}^{\text{img}}) &= \alpha \hat{x}_i^{img} + (1 - \alpha) \hat{x}_j^{img} \\ &= \text{IM}(\mathbf{x}) + [\alpha \delta_i + (1 - \alpha) \delta_j] \\ &\neq \text{IM}(\mathbf{x}) + \operatorname*{arg\,max}_{\delta \in \Delta} \mathcal{L}_{\alpha}^{mix}(\text{IM}(\mathbf{x}) + \delta), \end{split} \tag{9}$$

In order to maximize the loss to create a strong attack on interpolated images that can fool the classifier, the perturbation step should be the final step to ensure that the resulting adversarial samples are optimized to fool the classifier. Therefore, we consider the following *Robust Mixup strategy*. Suppose we have the interpolated images in image space $\mathrm{IM}(\mathbf{x})$ and the interpolated latent vectors $\mathrm{IM}(\mathbf{z})$. Then we apply the PGD attack on $\mathrm{IM}(\mathbf{x})$ and DPGD on $\mathrm{IM}(\mathbf{z})$. In

Algorithm 1 Interpolated Joint Space Adversarial Training (IJSAT)

Input: Training set \mathcal{D}_{tr} , classifier f_{θ} , generative model G, parameter of Beta distribution τ .

```
1: Initialize f_{\theta}
 2: for epoch = 1, ..., k do
                Sample \{x_i, y_i, z_i\}, \{x_j, y_j, z_j\} \sim \mathcal{D}_{tr}
 3:
                Sample \alpha \sim Beta(-\tau, \tau)
 4:
                IM(\mathbf{x}) = \alpha x_i + (1 - \alpha)x_i
                                                                                      \triangleright Input Mixup in X
 5:
                \begin{split} & \text{IM}(\mathbf{y}) = \alpha y_i + (1 - \alpha) y_j \\ & \mathbf{z}^{mixup} = G^{-1}(\text{IM}(\mathbf{x})) \end{split}
 6:
 7:
                \hat{x} = \text{JSA}(\mathbf{z}^{mixup}, \widetilde{\text{IM}}(\mathbf{y}))
                                                                                                          ⊳ Run JSA
 8:
                 \begin{array}{l} \mathcal{L}_{\alpha}^{mix}(\hat{x}) = \alpha \mathcal{L}(f_{\theta}(\hat{x},y_i)) + (1-\alpha)\mathcal{L}(f_{\theta}(\hat{x},y_j)) \\ g \leftarrow \nabla_{\theta}\mathcal{L}_{\alpha}^{mix} & \rhd \text{ Gradient of the mixup los} \end{array} 
 9:
                                                                  ⊳ Gradient of the mixup loss
10:
                \theta \leftarrow Step(\theta, g)
                                                                                   ▶ Update parameters
11:
                                                                                        using gradients g
```

12: end for

other words, we use (6) to iteratively maximize the loss, i.e.

$$\begin{split} \delta_{k+1} &= \hat{\epsilon} \cdot sign\left(\nabla_{\delta_k} \mathcal{L}_{\alpha}^{mix}(\mathtt{IM}(\mathbf{x})_k + \delta_k)\right) \\ &= \hat{\epsilon} \cdot sign\left[\nabla_{\delta_k} \left(\alpha \mathcal{L}(f_{\theta}(\mathtt{IM}(\mathbf{x})_k + \delta_k), y_i) \right.\right. \\ &\left. + (1 - \alpha) \mathcal{L}(f_{\theta}(\mathtt{IM}(\mathbf{x})_k + \delta_k), y_j)\right)\right]. \end{split} \tag{10}$$

The interpolated step followed by perturbation will ensure that the resultant images are optimized and generate a stronger attack.

5. Interpolated Joint Space Adversarial Training

Joint Space Attack can be used to harden a classifier against both seen and unseen attacks. The intuition, which we verify in Section 6, is that on-manifold adversarial samples improve the generalization of the classifier given exact manifold assumption holds according to [33]. JSA also lies within NPTM [28] which has been shown to be a comprehensive threat model and provide good robustness to unseen attacks. On the other hand, the image space perturbation in JSA can help the classifier to defend L_p attacks such as FGSM, PGD, and Auto Attacks. Combined with the proposed Robust Mixup strategy, we have the following *Interpolated Joint Space Adversarial Training (IJSAT)* framework:

IJSAT Optimization:
$$\min_{\theta} \left\{ \max_{\delta \in \Delta, \lambda \in \Lambda} \mathcal{L}_{\alpha}^{mix} \Big(G \big(G^{-1} (\text{IM}(x)) + \lambda \big) + \delta \Big) \right\}$$
(11)

The detailed algorithm is described in Algorithm Block 1.

6. Experiments

6.1. Implementation Details

Dataset: We evaluate the proposed method on the CIFAR-10, CIFAR-10-C [18], CIFAR-100 and OM-ImageNet [33] datasets. In the OM-ImageNet dataset, all images are from ImageNet and projected by StyleGAN. In other words, all images are on-manifold and have the corresponding latent vectors. The CIFAR-100 results are shown in supplementary material.

Models: For CIFAR-10 and CIFAR-100, we use ResNet-18. We follow [58] to have batch size 128 with 120 epochs. We use the SGD optimizer with setting initial learning rate to 0.1, momentum to 0.9 and weight decay to 2×10^{-4} .The learning rate drops by 0.1 at the 75-th, 90-th and 100th epochs. We set $\epsilon = 8/255$, $\epsilon_{iter} = 2/255$ for image space attacks and $\eta = 0.02$, $\eta_{iter} = 0.005$ for latent space attacks with 10 iteration steps. For OM-ImageNet, we follow [33] to use ResNet-50 [17] and train the classifier with 20 epochs. We use the SGD optimizer with the cyclic learning rate scheduling strategy in [53], momentum 0.9, and weight decay 5×10^{-4} . We set $\epsilon = 4/255$, $\epsilon_{iter} = 1/255$ for image space attacks and $\eta = 0.02$, $\eta_{iter} = 0.005$ for latent space attacks with 5 iteration steps. For input mixup, we use $\tau = 0.1$ for the random scalar, i.e. $\alpha \sim \text{Beta}(-\tau, \tau)$. For TRADES and MART, we use $\beta = 6.0$ for the KLdivergence loss. Different training setting will be explicitly mentioned otherwise. For all models trained by the proposed method, we use GLOW [22] as the generator.

6.2. Evaluation Settings

We evaluate our method in three aspects: (I) Standard Accuracy; (II) Robustness and (III) Generalization.

Standard Accuracy: We compare our model with **Normal Training**, **VAE-GAN** [47]–on-manifold adversarial samples using VAE-GAN, **Cutout** [10]-data augmentation with input masking, **Mixup** [57]-data augmentation with interpolated images, **Randomized-LA** and **Adversarial-LA** [56]-on-manifold adversarial samples using GLOW in CIFAR-10 dataset.

Robustness: We compare our model with L_{∞} **AT** [34], **DMAT** [33]-on-manifold adversarial training using Style-GAN, **IAT** [29]-interpolated adversarial training using Input Mixup, **TRADES** [58]-adversarial training using regularized surrogate loss to encourage smooth output and **MART** [51]-adversarial training that explicitly differentiates the misclassified and correctly classified examples in CIFAR-10, CIFAR-100 and OM-ImageNet dataset. For CIFAR-10 and CIFAR-100, we use PGD-20, Auto-Attack [9], which is an ensemble of four diverse attacks and the proposed JSA attack as the seen attacks. For unseen attacks, we use Elastic, JPEG and L_2 from [21]. For OM-ImageNet,

Table 1. Classification accuracy against various attacks applied to CIFAR10 dataset. Bold values indicate the best performance.

Method	Standard	PGD^{20}	AA	JSA^{50}	Elastic	JPEG	L_2	Avg
Normal Training	94.69	0.00	0.00	0.00	29.61	0.00	0.00	17.76
AT [PGD-5] [34]	84.15	49.85	44.71	45.71	45.16	26.71	18.75	45.01
DMAT [33]	82.77	45.01	34.08	36.78	56.72	38.42	28.6	46.05
IAT [29]	86.45	47.88	41.27	40.17	59.09	31.15	22.97	47.00
TRADES [58]	82.86	53.88	48.87	48.27	54.73	32.55	22.72	49.13
MART [51]	82.81	53.25	45.58	46.73	56.48	28.4	20.4	47.67
IJSAT (ours)	83.16	53.68	47.58	47.43	59.74	30.01	23.18	49.25

we follow [33] to have a total of eleven attacks.

Generalization: We compare our model with L_{∞} **AT**, L_2 **AT**, **Fast PAT** [28]-adversarial training using perceptual adversarial samples, **AdvProp** [55]-uses separate auxiliary batch norm for adversarial samples and **RLAT** [23]-relaxation of the LPIPS adversarial training in CIFAR-10-C dataset [18], which is a CIFAR-10 dataset with a total of fifteen common image corruptions.

6.3. Main Results

CIFAR-10 Robustness: We show the robustness results on CIFAR-10 in Table 1. First, by comparing the baseline AT method and our proposed method IJAST, we observe significant improvement in robustness against all six attacks. For DMAT, since it uses a GAN model to project the image to obtain the latent vectors, which cannot reconstruct the images exactly, robustness against off-manifold attacks drops as it does not generalize well without exact manifold assumption. Surprisingly, DMAT gains robustness to unseen attacks because of inexact image reconstruction (See Fig. 1(c)). IAT has the best standard accuracy as it uses Input Mixup and trains with clean images. However, we observe robustness against off-manifold attacks drops as there is a trade-off between standard accuracy and robustness. The proposed IJSAT has a comparable robustness against PGD-20 attacks with TRADES and MART while TRADEs achieves the best performance in Auto Attack and IJSAT achieves the second best. Unlike TRADES, which uses a surrogate function, and MART, which uses the boosted cross-entropy function to gain robustness, IJSAT only uses adversarial samples crafted from the proposed JSTM to achieve similar robustness gain while achieving the best standard accuracy. TRADES and MART can be further improved with IJSAT as shown in Sec. 6.6. Overall, IJSAT achieves the best average performance.

OM-ImageNet Robustness: To test our method with high-resolution images, we evaluate our methods with OM-ImageNet. Since every image has the corresponding latent vectors in the OM-ImageNet dataset, we do not need to use the Flow-based model to compute the latent vectors to ensure exact manifold assumption. The results are in Table 3. For off-manifold attacks, TRADES, MART, and IJSAT generally achieve better performance than oth-

Table 2. Left: Standard accuracy on CIFAR-10. Right: Common corruption accuracy on CIFAR-10-C. Bold values indicate the best performance in that section.

Method	Standard	Method	Corrupted
Normal Training	95.2	Normal Training	74.3
VAE-GAN [47]	94.2	L_{∞} AT	82.7
Cutout [10]	96.0	L_2 AT	83.4
Input Mixup [57]	95.9	Fast PAT [28]	82.4
Randomized-LA [56]	96.3	AdvProp [55]	82.9
Adversarial-LA [56]	96.6	RLAT [23]	84.1
IJSAT (ours)	96.9	IJSAT (ours)	84.6

ers. IJSAT performs the best as the JSA adversarial samples provide significant robustness to off-manifold attacks. For on-manifold robustness, since only DMAT and IJSAT consider on-manifold adversarial samples, they have significantly better on-manifold robustness than others. Among these two models, IJSAT has better on-manifold robustness than DMAT. For novel attacks, DMAT and IJSAT achieve generally better performance than the others. This is consistent with [33] that on-manifold adversarial samples improve generalization to novel attacks. Also, the mixup strategy improves generalization. From Table 3, IAT is consistently better than AT [PGD-5] in terms of robustness to novel attacks. Therefore, the proposed Robust Mixup strategy also boosts generalization performance, and hence IJSAT achieves the best robustness to novel attacks.

Standard Accuracy: We compare the proposed method to other data augmentation methods, and the results are shown in Table 2. Since image space perturbation decreases standard accuracy, we train a model by IJSAT with no image space perturbation, and other hyperparameters follow [56]. This can be used as data augmentation. Note that although both Adversarial-LA and the proposed method use GLOW to craft on-manifold adversarial samples, Adversarial-LA uses L_2 norm in the latent space and does not have a mixup strategy. In contrast, the proposed IJSAT uses L_∞ norm in the latent space with the proposed Robust Mixup strategy. Therefore, IJSAT achieves the best standard accuracy.

Generalization: We use CIFAR-10-C to demonstrate the generalization power of IJSAT. To achieve a good performance in CIFAR-10-C, we train our model with image space budget $\epsilon=1/255$ and $\epsilon_{iter}=\epsilon/4$ and other hyperparameters follow [23]. We show the results in Table 2. Both Fast PAT and RLAT lie within NPTM and use perceptual adversarial samples to train the model, and hence they generalize well to corrupted images. From Lemma 1, we know that the latent space perturbation in JSA samples lies within NPTM. On the other hand, JSA samples also include image space perturbation, and hence IJSAT achieves the best result.

Table 3. Classification accuracy against different attacks applied to OM-ImageNet test set. Bold values indicate the best performance in that section.

Method	Standard	FGSM	PGD-50	MIA	OM-PGD-50	Fog	Snow	Elastic	Gabor	JPEG	L_2
Normal Training	74.72	2.59	0.00	0.00	0.26	0.03	0.06	1.20	0.03	0.00	1.7
AT [PGD-5] [34]	73.31	48.02	38.88	39.21	7.23	19.76	46.39	50.32	50.43	10.23	41.98
DMAT [33]	77.96	49.12	37.86	37.65	20.53	31.78	51.19	56.09	51.61	14.31	51.36
IAT [29]	76.75	48.33	37.58	38.05	9.41	27.07	48.36	52.51	51.02	13.33	43.24
TRADES [58]	72.34	53.29	47.76	47.84	10.04	26.86	51.13	55.57	55.79	10.28	46.75
MART [51]	72.86	52.28	45.43	45.62	8.61	25.34	51.00	54.40	54.27	8.95	44.63
IJSAT (ours)	73.72	56.55	50.85	51.07	23.92	32.7	57.23	59.95	59.82	22.47	56.40

6.4. Ablation Studies

Since IJSAT has multiple components, we demonstrate the improvements using the CIFAR-10 dataset, one component at a time. The results are shown in Table 4.

6.4.1 Importance of Having Exact Manifold Information

To demonstrate the importance of having exact manifold information, we compare the on-manifold adversarial image crafted from GAN and flow-based models. We train a GAN model with CIFAR-10 and use it to craft JSA samples. Then we train a model with them, denoted as AT [JSA¹⁰-GAN]. In other words, the only difference between AT [JSA¹⁰-GAN] and AT [JSA¹⁰] is that the former uses a GAN as the generator while the latter uses the Flow-based model. In Table 4, we observe a significant improvement with standard accuracy ($\sim 10\% \uparrow$), and robustness of L_{∞} attacks $(\sim 14\% \uparrow)$ and unseen attacks $(\sim 9\% \uparrow)$ for AT [JSA¹⁰]. As JSA¹⁰ samples have the exact manifold information, the on-manifold adversarial samples preserve the details of the images while JSA¹⁰-GAN does not. As shown in Fig. 1(c), we observe a large difference between the original image and the projected image. Even though the projected image has similar semantic details, the projected image makes the classifier hard to generalize well when natural images are evaluated.

6.4.2 JSA Adversarial Samples Improves Robustness Significantly

To demonstrate the robustness gain whilst training with JSA samples, we train an AT model with JSA samples and compare them with standard AT, denoted as AT [PGD¹⁰] and AT [JSA¹⁰] respectively. From Table 4, we observe significant improvement with robustness of L_{∞} attacks ($\sim 3\% \uparrow$) and unseen attacks ($\sim 7\% \uparrow$) AT [JSA¹⁰]. Since the only difference between these two models is the adversarial sample, this indicates that JSA samples provide more robustness to the trained model than L_{∞} samples.

Since the JST model considers image and latent space perturbations, the resultant perturbations will have a larger attack budget. To investigate whether the success of IJAST is due to adversarial training with a large attack budget, we

Table 4. Ablations studies of IJSAT. Classification accuracy against different attacks applied to CIFAR-10. Bold values indicate the best performance in that section.

Method	Standard	PGD^{20}	AA	JSA^{50}	Elastic	JPEG	L_2	Avg
Normal Training	94.69	0	0	0	29.61	0	0	17.76
AT [PGD ¹⁰]	84.15	49.85	44.71	45.71	45.16	26.76	18.75	45.01
$\hookrightarrow \epsilon = 16/255$	68.91	52.78	47.32	47.95	47.09	32.97	27.02	46.29
$\hookrightarrow \epsilon = 32/255$	37.11	31.67	28.91	30.14	21.67	10.06	11.06	14.26
AT [JSA ¹⁰ -GAN]	76.43	47.04	43.10	43.82	39.35	18.63	26.09	42.07
AT [JSA ¹⁰]	82.75	53.15	47.47	47.10	59.67	28.79	22.69	48.80
+ mixup	83.08	53.12	47.59	47.04	59.65	28.56	23.56	48.94
IJSAT	83.16	53.68	47.58	47.43	59.74	30.01	23.18	49.25

conduct experiments with models trained with larger attack budgets. We train an AT model with image space budget $\epsilon=16/255$ and $\epsilon=32/255$ and compare their robustness against both L_{∞} and unseen attacks. We compare them with the proposed AT [JSA 10], using $L_{\infty}=8/255$ as the attack budget in image space and $L_{\infty}=0.002$ in latent space. From Table 4, we observe that the standard accuracy drops when the models are trained with a larger L_{∞} budget. The AT [PGD 10 , 16/255] has similar L_{∞} robustness with AT [JSA 10], which AT [JSA 10] is slightly better. However, this model has a 14% drop in standard accuracy compared with AT [JSA 10]. It is even worse when we increase the budget to 32/255. This experiment shows that the robustness gain of JSA samples does not merely rely on larger attack budgets.

6.4.3 Robust Mixup Further Boosts Standard Accuracy, Robustness and Generalization

Mixup as a data augmentation method usually helps in classifier training. However, crafting the adversarial samples and then doing the mixup will negatively impact the robustness. We denote this model as AT [JSA¹⁰]-mixup. From Table 4, using mixup in AT [JSA¹⁰] cannot guarantee improving robustness. This is because the interpolated perturbations need not be the optimized perturbations to the interpolated images (See Eq. (9)). When applying Robust Mixup (denoted as IJSAT), both standard accuracy and robustness are further improved. The perturbation step as the final step ensures that the adversarial sample maximizes the cross-entropy loss and fools the classifier. Training with these strong adversarial samples results in improving the ro-



Figure 4. Visualization of adversarial samples from JSA. Top: Original. Middle: JSA. Bottom: Magnified difference.

Table 5. Classification accuracy against different attacks applied to CIFAR-10 dataset.

Method	Standard	$ PGD^{20} $	AA	Elastic	JPEG	L_2	Avg
AT [34]	84.15	49.85	44.71	45.16	26.76	18.75	49.76
AT [34] + JSA	82.75	53.15	47.47	59.67	28.79	22.69	48.80
Difference	↓1.4	↑3.3	↑2.76	↑14.51	↑2.03	↑3.94	↑3.79
TRADES [58]	82.86	53.88	48.87	54.73	32.55	23.72	53.79
TRADES $[58]$ + JSA	82.70	54.22	49.10	58.66	32.55	25.18	54.68
Difference	↓0.16	↑0.34	↑0.23	↑3.93	0	↑1.46	↑0.89
MART [51]	82.81	53.25	45.58	56.48	28.4	20.47	52.36
MART[51] + JSA	81.33	54.28	46.53	59.15	30.3	24.28	53.64
Difference	↓1.48	↑1.03	↑0.95	↑2.67	↑1.9	↑3.81	↑1.28

bustness.

We plot the robust accuracy during training in Fig. 2. We can observe that IJSAT achieves the best robustness. Moreover, without mixup, the robustness of the model would decay after learning rate changes (at 75^{th} epoch). Input Mixup can help slightly (green line), while the proposed Robust Mixup can further improve robustness after learning rate changes (blue line), which reduces robust-overfitting.

6.5. Joint Space Attacks

In Table 4, we show the accuracy of different models against JSA. JSA is a strong attack, and it achieves similar results as AA. TRADES achieves the best while the proposed IJAST is the second best. Visualization results of JSA samples are shown in Fig. 1. For the PGD attack, the perturbations are noise covering the entire image. For OM-PGD (GAN), the projection step in GAN leads to a significant difference between the adversarial image and the original image. For OM-PGD (Flow), since the Flow-based model crafts the perturbation, it preserves the semantic information but cannot provide robustness to L_p attacks. For JSA, we observe that both image and latent space perturbations provide robustness to L_p and unseen attacks. We empirically show the JSA perturbation would not change the semantic meaning of the images (See Fig. 4).

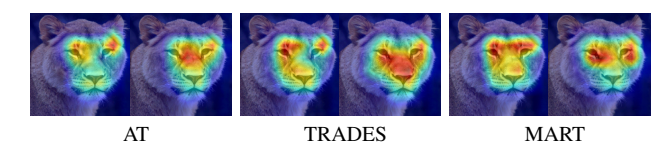


Figure 5. Visualization of CAM for different methods with and without JSA against PGD attack. Left: Original AT method. Right: AT method with JSA.

6.6. Applying JSA in Other Adversarial Training Methods

JSA also can be combined with existing AT methods. The results for CIFAR-10 dataset are shown in Table 5. For AT, TRADES, and MART, the robustness for L_{∞} , L_2 , on-manifold, and non- L_p attacks is improved after applying JSA. This demonstrates the flexibility of applying JSA adversarial to existing adversarial training methods and enhance robustness. To understand how JSA improves robustness, we can use a class activation map (CAM) to obtain a good visual explanation. In this paper, we use GRAD-CAM [45] to visualize. The CAM results are shown in Fig. 5. For the existing adversarial training method, the heatmap has a higher confidence score and overlaps more with the semantic meaningful region (the face of the leopard) when JSA is used.

7. Conclusion and Discussion

In this paper, we propose a novel threat model, JSTM, which considers both image and latent space perturbations. Under this threat model, we propose JSA and use it to train the classifier. This overcomes the drawbacks of AT not being able to generalize well to unseen attacks and lack of robustness of on-manifold adversarial training to L_p attacks. To ensure JSA samples generalize well to real datasets, we exploit the invertibility of the Flow-based model to make the exact manifold assumption holds. To further improve robustness and prevent overfitting, we propose the Robust Mixup strategy. Our extensive experiments show that IJSAT strikes a good balance among standard accuracy, robustness to seen attacks, and generalization to unseen attacks. Moreover, we demonstrate the flexibility of IJSAT that it can serve as a data augmentation method to improve standard accuracy and assist existing AT methods achieve better performance.

Future research direction can address the common drawback of on-manifold adversarial training, including DMAT, Adversarial-LA, and the proposed IJSAT. All of them require an additional generator to capture the data manifold and craft adversarial samples. One possible way to drop the generator is to use the feature map of the classifier as the latent space and generate the on-manifold adversarial samples, using the Invertible ResNet [4].

Acknowledgement

This work was supported by the DARPA GARD Program HR001119S0026-GARD-FP-052.

References

- [1] Vegard Antun, Francesco Renna, Clarice Poon, Ben Adcock, and Anders C Hansen. On instabilities of deep learning in image reconstruction and the potential costs of AI. *Proceedings of the National Academy of Sciences*, 2020. 1
- [2] Anish Athalye, Nicholas Carlini, and David Wagner. Obfuscated gradients give a false sense of security: Circumventing defenses to adversarial examples. In *International Conference on Machine Learning*, pages 274–283, 2018. 1
- [3] Anish Athalye, Logan Engstrom, Andrew Ilyas, and Kevin Kwok. Synthesizing robust adversarial examples. In *Inter-national Conference on Machine Learning*, pages 284–293, 2018.
- [4] Jens Behrmann, Will Grathwohl, Ricky T. Q. Chen, David Duvenaud, and Joern-Henrik Jacobsen. Invertible residual networks. In Kamalika Chaudhuri and Ruslan Salakhutdinov, editors, *Proceedings of the 36th International Conference on Machine Learning*, volume 97 of *Proceedings of Machine Learning Research*, pages 573–582, Long Beach, California, USA, 09–15 Jun 2019. PMLR. 8
- [5] Nicholas Carlini and David Wagner. Towards evaluating the robustness of neural networks. In *IEEE Symposium on Secu*rity and Srivacy (SP), pages 39–57. IEEE, 2017. 1
- [6] Yanzhi Chen, Renjie Xie, and Zhanxing Zhu. On breaking deep generative model-based defenses and beyond. In *International Conference on Machine Learning*, 2020. 2
- [7] Ping-Yeh Chiang, Renkun Ni, Ahmed Abdelkader, Chen Zhu, Christoph Studor, and Tom Goldstein. Certified defenses for adversarial patches. *arXiv preprint arXiv:2003.06693*, 2020. 1
- [8] Jeremy Cohen, Elan Rosenfeld, and Zico Kolter. Certified adversarial robustness via randomized smoothing. In *International Conference on Machine Learning*, pages 1310–1320, 2019.
- [9] Francesco Croce and Matthias Hein. Reliable evaluation of adversarial robustness with an ensemble of diverse parameter-free attacks. In *ICML*, 2020. 5
- [10] Terrance DeVries and Graham W Taylor. Improved regularization of convolutional neural networks with cutout. arXiv preprint arXiv:1708.04552, 2017. 5, 6
- [11] Laurent Dinh, David Krueger, and Yoshua Bengio. NICE: non-linear independent components estimation. In Yoshua Bengio and Yann LeCun, editors, 3rd International Conference on Learning Representations, ICLR 2015, San Diego, CA, USA, May 7-9, 2015, Workshop Track Proceedings, 2015. 3, 11
- [12] Laurent Dinh, Jascha Sohl-Dickstein, and Samy Bengio. Density estimation using real NVP. In 5th International Conference on Learning Representations, ICLR 2017, Toulon, France, April 24-26, 2017, Conference Track Proceedings. OpenReview.net, 2017. 3

- [13] Alhussein Fawzi, Hamza Fawzi, and Omar Fawzi. Adversarial vulnerability for any classifier. In *Advances in Neural Information Processing Systems*, 2018. 1
- [14] Partha Ghosh, Arpan Losalka, and Michael J Black. Resisting adversarial attacks using Gaussian mixture variational autoencoders. In *Proceedings of the AAAI Conference on Artificial Intelligence*, volume 33, pages 541–548, 2019.
- [15] Ross Girshick. Fast R-CNN. In International Conference on Computer Vision (ICCV), 2015.
- [16] Ian J. Goodfellow, Jonathon Shlens, and Christian Szegedy. Explaining and harnessing adversarial examples. *International Conference on Learning Representations*, 2015. 1
- [17] Kaiming He, Xiangyu Zhang, Shaoqing Ren, and Jian Sun. Deep residual learning for image recognition. In *Proceedings of the IEEE conference on computer vision and pattern recognition*, pages 770–778, 2016. 5
- [18] Dan Hendrycks and Thomas Dietterich. Benchmarking neural network robustness to common corruptions and perturbations. Proceedings of the International Conference on Learning Representations, 2019. 5, 6
- [19] G. Hinton, L. Deng, D. Yu, G. E. Dahl, A. Mohamed, N. Jaitly, A. Senior, V. Vanhoucke, P. Nguyen, T. N. Sainath, and B. Kingsbury. Deep neural networks for acoustic modeling in speech recognition: The shared views of four research groups. *IEEE Signal Processing Magazine*, 29(6):82–97, 2012. 1
- [20] Ajil Jalal, Andrew Ilyas, Constantinos Daskalakis, and Alexandros G Dimakis. The robust manifold defense: Adversarial training using generative models. arXiv preprint arXiv:1712.09196, 2017. 2
- [21] Daniel Kang, Yi Sun, Dan Hendrycks, Tom Brown, and Jacob Steinhardt. Testing robustness against unforeseen adversaries. arXiv preprint arXiv:1908.08016, 2019. 5
- [22] Diederik P. Kingma and Prafulla Dhariwal. Glow: Generative flow with invertible 1x1 convolutions. In Samy Bengio, Hanna M. Wallach, Hugo Larochelle, Kristen Grauman, Nicolò Cesa-Bianchi, and Roman Garnett, editors, Advances in Neural Information Processing Systems 31: Annual Conference on Neural Information Processing Systems 2018, NeurIPS 2018, December 3-8, 2018, Montréal, Canada, pages 10236–10245, 2018. 3, 5, 11
- [23] Klim Kireev, Maksym Andriushchenko, and Nicolas Flammarion. On the effectiveness of adversarial training against common corruptions. arXiv preprint arXiv:2103.02325, 2021. 6
- [24] Alex Krizhevsky, Geoffrey Hinton, et al. Learning multiple layers of features from tiny images. 2009. 11
- [25] Alex Krizhevsky, Ilya Sutskever, and Geoffrey Hinton. Imagenet classification with deep convolutional neural networks. Advances in Neural Information Processing Systems, 25, 01 2012.
- [26] Alexey Kurakin, Ian Goodfellow, and Samy Bengio. Adversarial examples in the physical world. arXiv preprint arXiv:1607.02533, 2016.
- [27] Cassidy Laidlaw and Soheil Feizi. Functional adversarial attacks. In Advances in Neural Information Processing Systems (NeurIPS), 2019.

- [28] Cassidy Laidlaw, Sahil Singla, and Soheil Feizi. Perceptual adversarial robustness: Defense against unseen threat models. In *ICLR*, 2021. 2, 4, 5, 6
- [29] Alex Lamb, Vikas Verma, Juho Kannala, and Yoshua Bengio. Interpolated adversarial training: Achieving robust neural networks without sacrificing too much accuracy. In *Proceedings of the 12th ACM Workshop on Artificial Intelligence and Security*, pages 95–103, 2019. 2, 3, 4, 5, 6, 7, 11
- [30] Saehyung Lee, Hyungyu Lee, and Sungroh Yoon. Adversarial vertex mixup: Toward better adversarially robust generalization. In *Proceedings of the IEEE/CVF Conference on Computer Vision and Pattern Recognition*, pages 272–281, 2020. 2
- [31] Alexander Levine and Soheil Feizi. Robustness certificates for sparse adversarial attacks by randomized ablation. Association for the Advancement of Artificial Intelligence (AAAI), 2020. 1
- [32] Alexander Levine and Soheil Feizi. Wasserstein smoothing: Certified robustness against Wasserstein adversarial attacks. *International Conference on Artificial Intelligence and Statistics (AISTATS)*, 2020. 1
- [33] Wei-An Lin, Chun Pong Lau, Alexander Levine, Rama Chellappa, and Soheil Feizi. Dual Manifold Adversarial Robustness: Defense against Lp and non-Lp Adversarial Attacks. In Advances in Neural Information Processing Systems, 2020. 1, 2, 4, 5, 6, 7, 11, 12
- [34] Aleksander Madry, Aleksandar Makelov, Ludwig Schmidt, Dimitris Tsipras, and Adrian Vladu. Towards deep learning models resistant to adversarial attacks. *arXiv preprint arXiv:1706.06083*, 2017. 1, 2, 3, 5, 6, 7, 8, 11
- [35] Pratyush Maini, Eric Wong, and Zico Kolter. Adversarial robustness against the union of multiple perturbation models. In *International Conference on Machine Learning*, pages 6640–6650. PMLR, 2020. 4
- [36] Takeru Miyato, Toshiki Kataoka, Masanori Koyama, and Yuichi Yoshida. Spectral normalization for generative adversarial networks. *arXiv preprint arXiv:1802.05957*, 2018.
- [37] Tianyu Pang, Kun Xu, and Jun Zhu. Mixup inference: Better exploiting mixup to defend adversarial attacks. In *Interna*tional Conference on Learning Representations, 2019. 1, 2, 3
- [38] Omid Poursaeed, Tianxing Jiang, Harry Yang, Serge Belongie, and Ser-Nam Lim. Fine-grained synthesis of unrestricted adversarial examples, 2019. 2
- [39] Aditi Raghunathan, Jacob Steinhardt, and Percy S Liang. Semidefinite relaxations for certifying robustness to adversarial examples. In *Advances in Neural Information Processing Systems*, pages 10877–10887, 2018. 1
- [40] Aditi Raghunathan, Sang Michael Xie, Fanny Yang, John Duchi, and Percy Liang. Understanding and mitigating the tradeoff between robustness and accuracy. arXiv preprint arXiv:2002.10716, 2020. 2
- [41] Leslie Rice, Eric Wong, and Zico Kolter. Overfitting in adversarially robust deep learning. In *International Conference on Machine Learning*, pages 8093–8104. PMLR, 2020. 2

- [42] Kevin Roth, Yannic Kilcher, and Thomas Hofmann. The odds are odd: A statistical test for detecting adversarial examples. In *International Conference on Machine Learning*, pages 5498–5507, 2019. 1
- [43] Pouya Samangouei, Maya Kabkab, and Rama Chellappa. Defense-gan: Protecting classifiers against adversarial attacks using generative models. *arXiv preprint arXiv:1805.06605*, 2018. 1, 2
- [44] Lukas Schott, Jonas Rauber, Matthias Bethge, and Wieland Brendel. Towards the first adversarially robust neural network model on mnist. In *International Conference on Learn*ing Representations, 2018. 2
- [45] Ramprasaath R Selvaraju, Michael Cogswell, Abhishek Das, Ramakrishna Vedantam, Devi Parikh, and Dhruv Batra. Grad-cam: Visual explanations from deep networks via gradient-based localization. In *Proceedings of the IEEE international conference on computer vision*, pages 618–626, 2017. 8, 12
- [46] Yang Song, Rui Shu, Nate Kushman, and Stefano Ermon. Constructing unrestricted adversarial examples with generative models. In Advances in Neural Information Processing Systems (NeurIPS), 2018.
- [47] David Stutz, Matthias Hein, and Bernt Schiele. Disentangling adversarial robustness and generalization. In *The IEEE Conference on Computer Vision and Pattern Recognition* (CVPR), June 2019. 2, 5, 6
- [48] David Stutz, Matthias Hein, and Bernt Schiele. Confidencecalibrated adversarial training: Generalizing to unseen attacks. Proceedings of the International Conference on Machine Learning ICML, 2020. 1
- [49] Dimitris Tsipras, Shibani Santurkar, Logan Engstrom, Alexander Turner, and Aleksander Madry. Robustness may be at odds with accuracy. In *International Conference on Learning Representations (ICLR)*, 2019. 12
- [50] Vikas Verma, Alex Lamb, Christopher Beckham, Amir Najafi, Ioannis Mitliagkas, David Lopez-Paz, and Yoshua Bengio. Manifold mixup: Better representations by interpolating hidden states. In *International Conference on Machine Learning*, pages 6438–6447, 2019. 2, 3
- [51] Yisen Wang, Difan Zou, Jinfeng Yi, James Bailey, Xingjun Ma, and Quanquan Gu. Improving adversarial robustness requires revisiting misclassified examples. In *International Conference on Learning Representations*, 2019. 5, 6, 7, 8, 11
- [52] Eric Wong and Zico Kolter. Provable defenses against adversarial examples via the convex outer adversarial polytope. In *International Conference on Machine Learning*, pages 5286–5295, 2018.
- [53] Eric Wong, Leslie Rice, and J. Zico Kolter. Fast is better than free: Revisiting adversarial training. In *International Conference on Learning Representations*, 2020. 5
- [54] Chang Xiao, Peilin Zhong, and Changxi Zheng. Resisting adversarial attacks by k-winners-take-all. arXiv preprint arXiv:1905.10510, 2019.
- [55] Cihang Xie, Mingxing Tan, Boqing Gong, Jiang Wang, Alan L Yuille, and Quoc V Le. Adversarial examples improve image recognition. In *Proceedings of the IEEE/CVF*

- Conference on Computer Vision and Pattern Recognition, pages 819–828, 2020. 6
- [56] Oğuz Kaan Yüksel, Sebastian U Stich, Martin Jaggi, and Tatjana Chavdarova. Semantic perturbations with normalizing flows for improved generalization. In *ICML Workshop on In*vertible Neural Networks, Normalizing Flows, and Explicit Likelihood Models, 2021. 5, 6
- [57] Hongyi Zhang, Moustapha Cisse, Yann N Dauphin, and David Lopez-Paz. mixup: Beyond empirical risk minimization. In *International Conference on Learning Representa*tions, 2018. 2, 3, 5, 6
- [58] Hongyang Zhang, Yaodong Yu, Jiantao Jiao, Eric Xing, Laurent El Ghaoui, and Michael Jordan. Theoretically principled trade-off between robustness and accuracy. In *International Conference on Machine Learning*, pages 7472–7482, 2019. 2, 5, 6, 7, 8, 11
- [59] Richard Zhang, Phillip Isola, Alexei A Efros, Eli Shechtman, and Oliver Wang. The unreasonable effectiveness of deep features as a perceptual metric. In *Proceedings of the IEEE Conference on Computer Vision and Pattern Recognition*, pages 586–595, 2018. 11

A. Implementation Details

A.1. Normalizing Flows

To craft on-manifold adversarial samples by our proposed method Joint Space Attack (JSA), we need to first train a flow-based model. We use Glow [22] in this work. Different from NICE [11] and RealNVP [11], Glow consists of a series of steps of flow, combined in a multi-scale architecture. The multi-scale architecture can reduce the computational complexity of the flow-based model. For each step of the flow, it consists of actnorm, followed by an invertible 1×1 convolution layer and followed by a coupling layer. LU decomposition is used to calculate the weight matrix of the invertible 1×1 convolution. The number of levels of the Glow we trained is 4 and we have 8 steps of flow for each flow. For both CIFAR-10 [24] and OM-ImageNet [33] datasets, we train the flow-based model with the original image resolution.

A.2. DMAT with CIFAR-10

DMAT [33] requires to use on-manifold images to train the models. They construct an OM-ImageNet dataset and conduct experiments on it. However, if we want to use DMAT in CIFAR-10 dataset, we need to construct an OM-CIFAR10 dataset. Since we would like to have a low-dimensional latent representation, instead of using Style-GAN which has a high dimensional latent representation for Om-ImageNet dataset, we use Spectral Normalization for Generative Adversarial Networks (SNGAN) [36] as the generator since images only have $32 \times 32 \times 3$ dimensions in CIFAR10 dataset. With the trained SNGAN, we project the training set $\mathcal{D}^o_{tr} = \{x_i, y_i\}_{i=1}^N$ onto the learned manifold by

Table 6. Performance comparison between DMAT trained with approximated manifold (GAN) and exact manifold (Flow) evaluated with the CIFAR-10 dataset.

Method	Standard PGD ²⁰	AA JSA ⁵⁰ Elastic	JPEG	L ₂ Avg
DMAT [33] DMAT [33] + JSA Difference	86.49 49.58	34.08 36.78 56.72 43.37 42.09 59.71 ↑9.29 ↑5.31 ↑2.99	26.75	18.80 46.68

Table 7. Classification accuracy against various attacks applied to CIFAR100 dataset. Bold values indicate the best performance.

Method	Standard	PGD^{20}	AA	Elastic	JPEG	L_2	Avg
Normal Training	75.73	0.01	0	9.41	0	0.43	14.263
AT [PGD-5] [34]	57.72	25.62	22.08	28.37	15.37	10.45	26.60
DMAT [33]	59.99	22.49	19.34	28.25	12.56	8.71	25.22
IAT [29]	61.86	23.55	19.69	31.9	13.6	9.93	26.755
TRADES [58]	56.46	28.45	23.3	26.46	16.92	13.01	27.43
MART [51]	52.81	29.49	24.09	27.71	16.08	14.16	27.39
IJSAT (ours)	55.83	29.84	23.97	33.47	17.28	14.95	29.22

solving:

$$z_i = \underset{z}{\arg\min} \text{ LPIPS}(G(z), x_i) + ||G(z) - x_i||_1.$$
 (12)

where LPIPS is Learned Perceptual Image Patch Similarity [59]. The training set contains the projected image with the corresponding latent vectors and labels and the test set contains natural images with corresponding labels. In other words, all the test images are natural (off-manifold) images. All images are normalized into [0, 1], and data augmentations are used during training including random horizontal flipping and 32×32 random cropping with 4-pixel padding. Sample images of the OM-CIFAR10 dataset are shown in Fig. 6.

In Table 6, we observe a significant improvement with standard accuracy (3.72% \uparrow), and robustness of L_{∞} attacks (7% \uparrow) for DMAT+JSA. Since DMAT+JSA has the exact manifold information, the on-manifold adversarial samples preserve the details of the images while DMAT does not. The L_2 and JPEG robustness of DMAT is much better than that of DMAT-JSA as there is a large difference between the original image and the projected image.

B. CIFAR-100 Robustness

To test our method on a dataset with more classes, we evaluate our methods on CIFAR-100. The results are in Table 7. We observe similar results as in CIFAR-10: 1) IJSAT has the best overall results; 2) MART, TRADES, and IJSAT achieve comparable L_{∞} robustness; 3) IJSAT achieves the best unseen attack robustness.

C. Clean Accuracy and PGD-50 Robustness for Multiple Snapshots during Training

We evaluate the trained models using the PGD-50 for multiple snapshots during training. The results are pre-

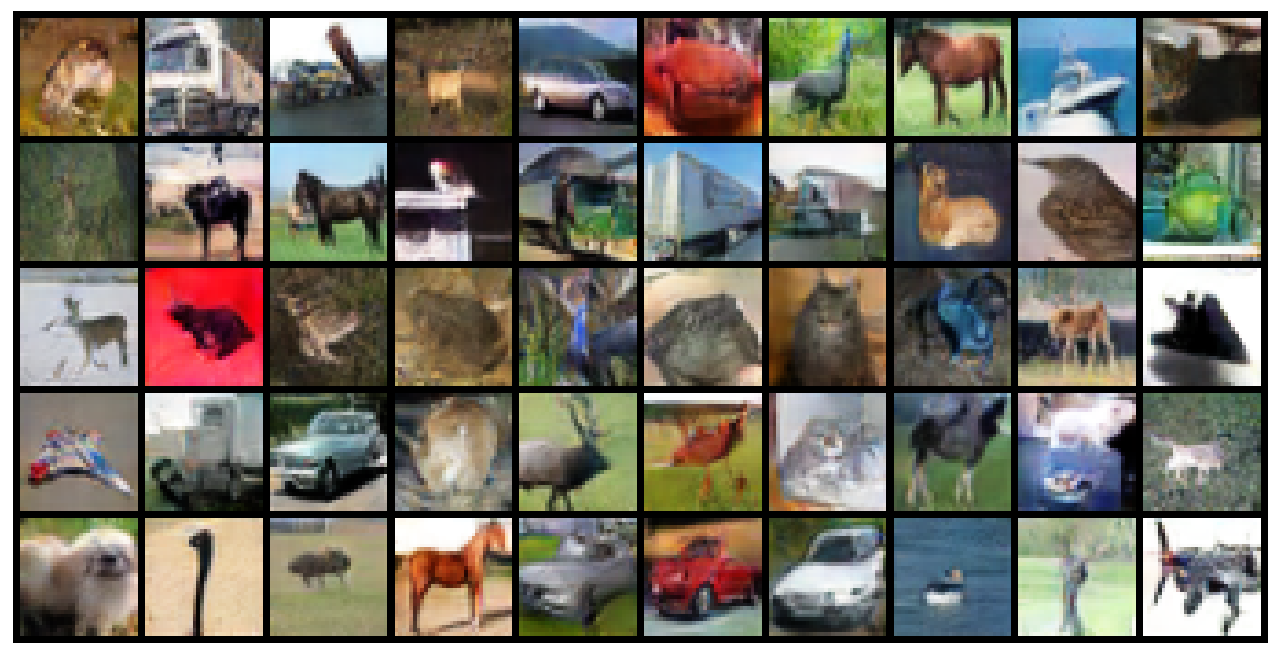


Figure 6. Sample images of OM-CIFAR10 dataset.

sented in Figure 7. We observe that (i) standard adversarial training leads to degraded standard accuracy (consistent with [49]), (ii) on-manifold adversarial samples (methods combined with JSA) improves standard accuracy (consistent with [33]), (iii) robustness to PGD attack improves when JSA is added during training and (iv) the improvement is the most significant when DMAT is combined with JSA, which justifies the importance of exact manifold.

D. JSA at different level of flow

As we mentioned in Sec. A.1, the Glow model we trained has multi-scale architecture. Mathematically, the latent vector is the following:

$$g^{-1}(x) = g_1^{-1} \circ g_2^{-1} \circ g_3^{-1} \circ g_4^{-1}(x) = (z_1, z_2, z_3, z_4) = z$$
(13)

where g is the flow-based model which consists of 4 levels. We perturb the whole latent vector z when we craft an adversarial sample from JSA. Instead of attacking the whole latent vector, we would like to visualize the adversarial samples when only one level of the latent vector is attacked. Mathematically,

$$\max_{\lambda_i \in \Lambda} \mathcal{L}(f_{\theta}(g(z_1, \dots, z_i + \lambda_i, z_4)), y_{\text{true}}), \tag{14}$$

for some flow level *i*. The visualization results are shown in Fig. 8. We can observe that the perturbation pattern changes from coarse to fine in semantic details. In other words, the perturbation pattern is similar to PGD or Gabor attack when

it is at level 1 and the perturbation becomes more similar to the subject (leopard in this example) when it is attacked at a higher level. Therefore, when the whole latent vector is attacked, all these perturbations will be accumulated and make This somehow explains why on-manifold adversarial samples from JSA could improve the robustness of various attacks.

E. Class Activation Map of JSTM

To understand how JSA samples improves standard accuracy and robustness, we can use a class activation map (CAM) to obtain a good visual explanation. In this paper, we use GRAD-CAM [45] to visualize. The CAM results are shown in Fig. 9. For the model with normal training, we can see the CAM is sparse on the semantic region even for the original image. With JSA, the CAM is more concentrated on the semantic region. For PGD, JSA, and Elastic attacks to model with normal training, these attacks break the classifier and make the CAM wrong. For normal training with JSA, it successfully defends JSA and Elastic attack and has a meaningful CAM while it is broken by PGD attack. For the existing adversarial training method, using JSA could have CAM more concentrated on the semantic regions (See the row AT and TRADE). This shows that using IA during training can help the classifier to concentrate more on the semantic regions than not using IA even both models classify correctly.

F. Additional Figures for JSA Images

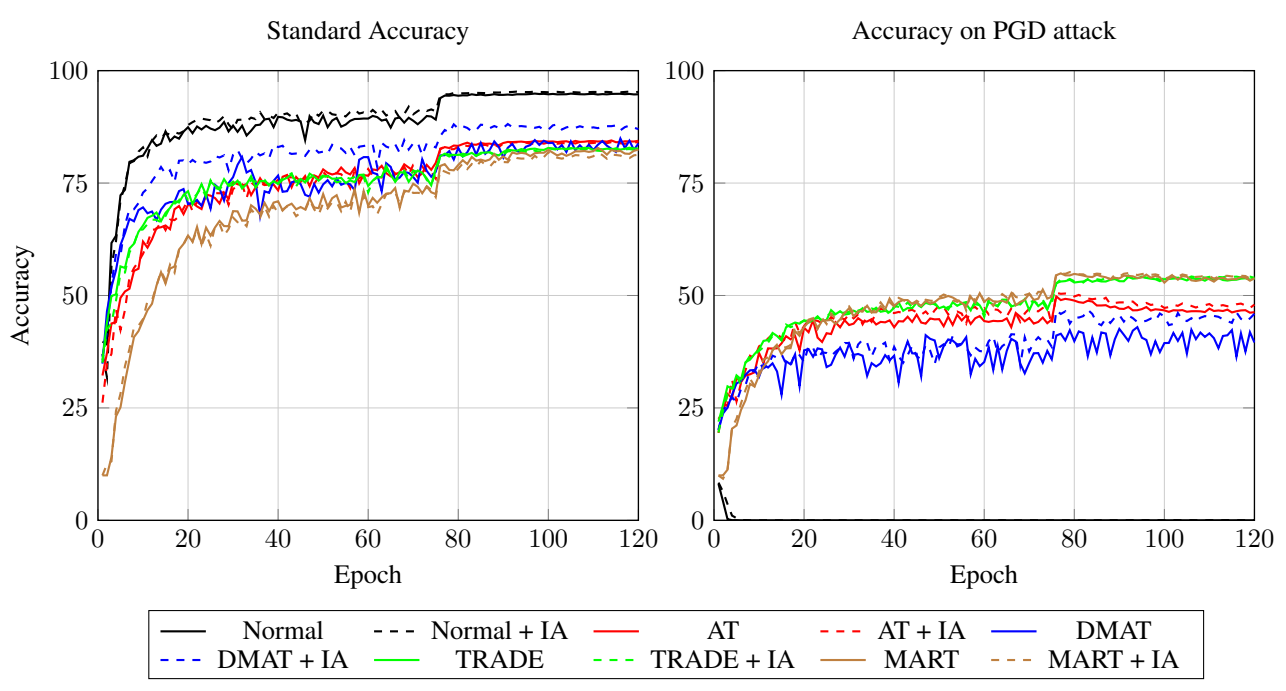


Figure 7. Clean accuracy and PGD-50 robustness during training with CIFAR-10 dataset. Using IA during improves both standard accuracy and robustness. Left: standard accuracy. Right: classification accuracy when the trained models are attacked by PGD attack.



 $\text{IA}\ (\eta=0.02)\ \text{at level 3}\ \ \text{IA}\ (\eta=0.04)\ \text{at level 3}\ \ \text{IA}\ (\eta=0.1)\ \text{at level 3}\ \ \text{IA}\ (\eta=0.02)\ \text{at level 4}\ \ \text{IA}\ (\eta=0.04)\ \text{at level 4}\ \ \text{IA}\ (\eta=0.1)\ \text{at level 4}\ \ \text{IA}\ (\eta=0.04)\ \text{at level 4}\ \ \text{IA}\ (\eta=0.1)\ \text{at level 4}\ \ \text{IA}\ (\eta=0.04)\ \ \text{I$

Figure 8. Visualization of adversarial samples from IA with various perturbation budgets at different flow levels. The differences are magnified for visualization purpose.

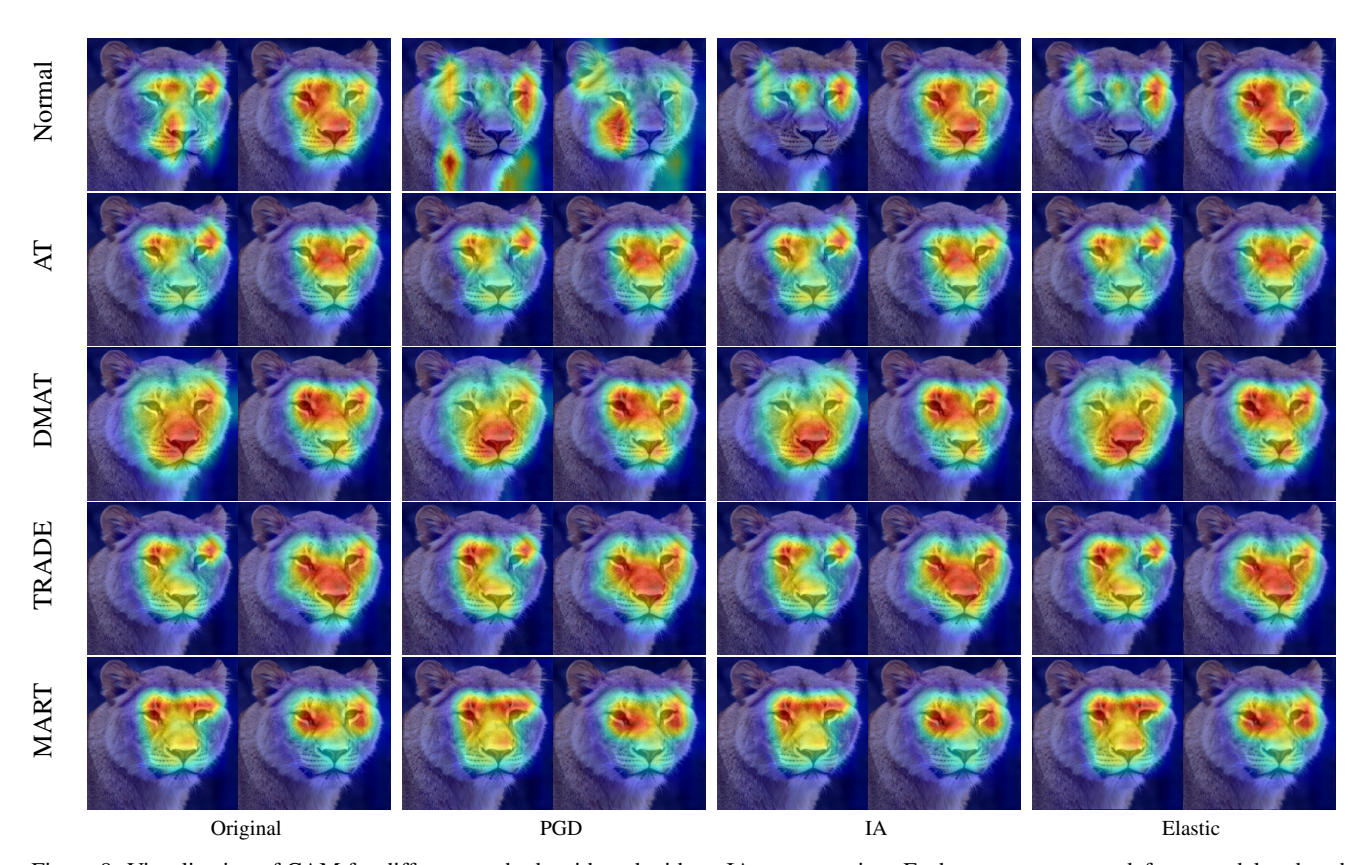


Figure 9. Visualization of CAM for different methods with and without IA augmentation. Each row represents a defense model and each column represents an attack. For each combination of attack and defense method, there are two images. The left one is the original method and the right one is that combined with IA. The heap map has a higher confidence score and overlap more with the semantic meaningful region (the face of teh leopard) when IA augmentation is used.

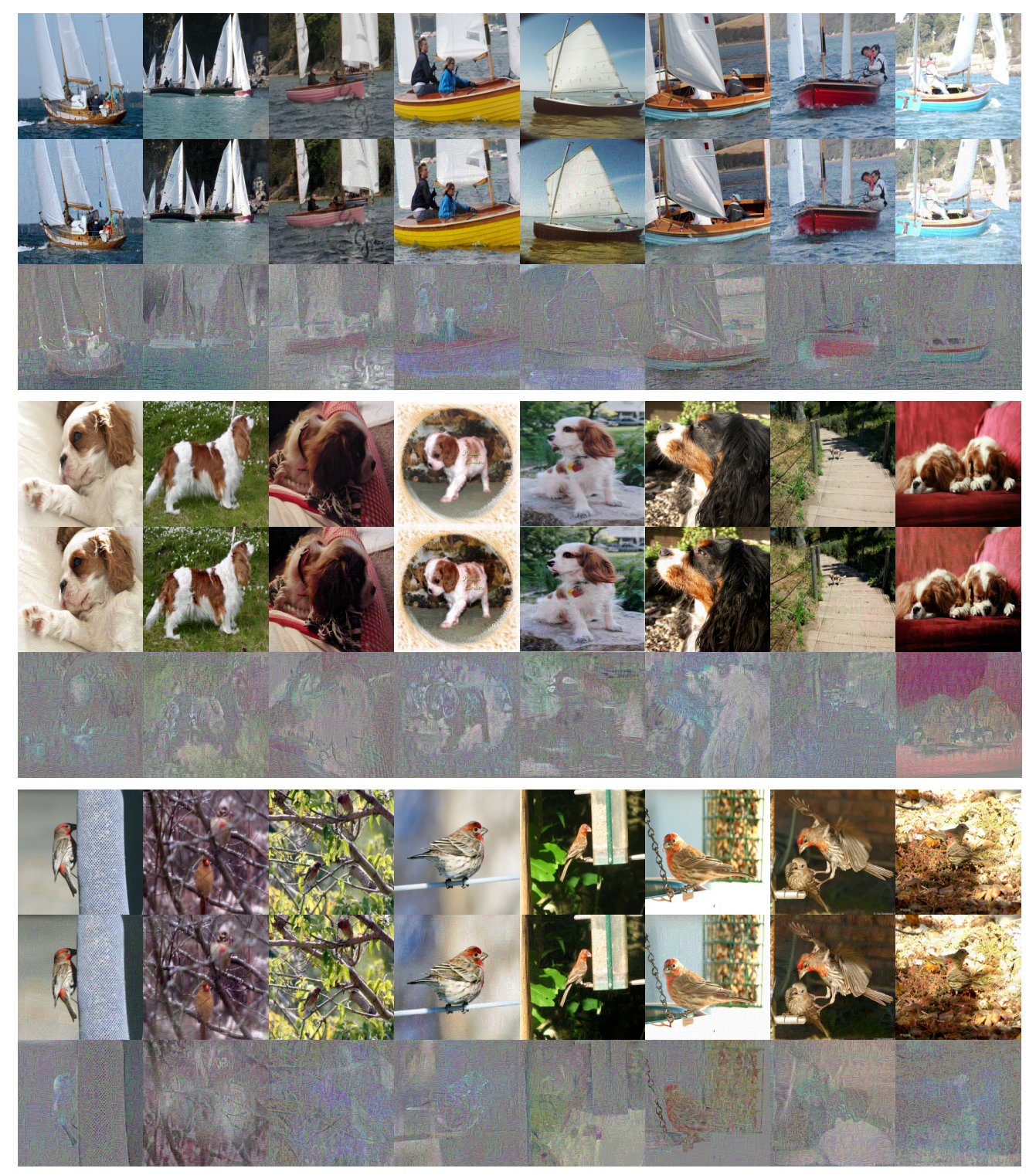


Figure 10. Visualization of adversarial samples from JSA. Top: Original. Middle: JSA. Bottom: Magnified difference.